International Journal of Innovative Computing, Information and Control
Volume **21**, Number **2**, April **2025**

ICIC International ©2025 ISSN 1349-4198
pp. **323–338**

GENERATIVE ADVERSARIAL NETWORKS FOR REMOTE SENSING IMAGE DEHAZING WITH COLOR FEATURE RESTORATION

Liquan Zhao[1], Yuqing Qin[1,*] and Yanfei Jia[2]

[1]Key Laboratory of Modern Power System Simulation and Control and Renewable Energy Technology
Ministry of Education
Northeast Electric Power University
No. 169, Changchun Road, Jilin 132012, P. R. China
zhaoliquan@neepu.edu.cn; *Corresponding author: 2202200363@neepu.edu.cn

[2]College of Electric and Information Engineering
Beihua University
No. 3999, Beijing Road, Jilin 132013, P. R. China
jiayanfei@beihua.edu.cn

Received June 2024; revised October 2024

Abstract. *Remote sensing images are often affected by atmospheric factors such as haze during the acquisition process, resulting in blurring and low contrast in the collected remote sensing images. This problem impacts the image quality, thereby affecting the analysis of remote sensing images. To mitigate the impact of haze on remote sensing images, a generative adversarial network is proposed. It comprises a generative network and an adversarial network. Firstly, a novel feature extraction module is designed to enhance the capability of extracting useful information from remote sensing images. It enables the network to focus more on regions with dense haze, allowing it to extract more important information while filtering out irrelevant details. Secondly, a residual attention module is designed which can allocate different weights based on varying haze density in the feature map. This module readjusts features outputted by the encoder, facilitating better image restoration. Thirdly, a multi-scale module is also incorporated to extract feature information across various image scales. Lastly, a color feature extraction module is designed to extract color features. The novel feature extraction module, residual attention module, multi-scale module, and color feature extraction module are utilized for constructing the generative network. Besides, an adversarial network is also designed to indirectly enhance the dehazing capability of the generative network. Synthetic and real datasets are used to test six different methods for dehazing remote sensing images, respectively. The proposed method achieves higher PSNR, SSIM, and lower MSE on the synthetic remote sensing dataset. On the other hand, it achieves lower PIQE, BRISQUE, and higher MetaIQA on the real remote sensing dataset. The proposed method has best performance in dehazing remote sensing images than other methods.*

Keywords: Generative adversarial network, Remote sensing image dehazing, Feature extraction module, Residual attention module, Multi-scale module, Color feature extraction module

1. **Introduction.** Remote sensing technology facilitates the acquisition of information regarding the Earth's surface through aerial and satellite methods. Remote sensing images enable us to comprehensively monitor, analyze, and understand various features and changes on Earth. High-quality remote sensing images are crucial for gaining in-depth insights into the characteristics and changes of the Earth's surface. Remote sensing images find wide applications in natural disaster investigation [1], environmental monitoring and

DOI: 10.24507/ijicic.21.02.323

assessment [2], urban dynamic monitoring [3], and urban planning [4], among other fields [5]. High-quality remote sensing images can provide more precise and accurate surface information, aiding in the identification of objects, detection of changes, and quantitative analysis. Additionally, high-quality remote sensing images can ensure the reliability and authenticity of subsequent research results. Therefore, ensuring the quality of remote sensing images is paramount. However, when acquiring remote sensing images, they are often susceptible to haze interference [6]. This can result in blurry images with indiscernible details, consequently reducing the usability of remote sensing data. Thus, mitigating the impact of haze on remote sensing images and improving their quality is crucial [7]. Existing approaches to haze removal in remote sensing images can be broadly classified into three categories: image enhancement-based methods, prior information-based methods, and learning-based methods. Learning-based methods generally outperform other approaches regarding dehazing effectiveness and generalization capabilities. However, dehazed remote sensing images produced by learning-based methods still suffer from artifacts, color distortion, and loss of details.

To address these challenges, we designed a novel remote sensing image dehazing network based on Generative Adversarial Networks (GANs) aimed at enhancing the overall quality of remote sensing images. We tested the methods using both synthetic hazy remote sensing images and real hazy remote sensing images. For the synthetic images, the proposed model achieved the highest PSNR (33.4842) and SSIM (0.9854) values, along with the lowest MSE (0.0010) value. For the real images, the algorithm demonstrated the lowest PIQE (11.3699) and BRISQUE (29.5038) values, as well as the highest MetaIQA (0.2621) value. This indicates that the proposed model performs best in dehazing both synthetic and real hazy remote sensing images compared to other methods.

The main contributions of this paper are summarized as follows.

1) We designed a novel feature extraction module that consists of convolution, batch normalization, and attention module. It can extract more useful features while reducing redundant information interference. We designed a residual attention module with three branches. It can enable the network to focus on essential features and thereby enhancing feature utilization efficiency. We designed a multi-scale module that consists of dilated convolutions with different dilation rates, average pooling, maximum pooling and batch normalization. It can extract features from multiple scales. We designed a color feature extraction module with residual structure to additionally extract color features and reduce color distortion.

2) Based on the above designed modules, we designed a generative network with an encoder-decoder structure to realize remote sensing image dehazing. It mainly consists of encoder network, decoder network and color feature extraction module. The encoder network is used to extract texture information. The decoder network is used to extract edge information. We used two residual attention modules to transmit feature maps of different scales from the encoder to the decoder, and fused the feature maps of the same scale using concatenation. The fused features incorporate shallow network characteristics, reducing feature loss. The generative network not only removes haze but also preserves critical image details more effectively, minimizes artifacts, and significantly enhances the overall quality of remote sensing images.

3) We developed an adversarial network that distinguishes between real and generated outputs of the generative network for dehazing remote sensing images. The adversarial network consists of three same modules. Each module consists of convolutions, batch normalization, dropout, and LeakyReLU activation. Through the interplay between the adversarial network and the generative network, the dehazing capability of the generative network for remote sensing images can be indirectly improved.

This section discusses the background of image dehazing, highlighting the contributions and significance of this research, as well as presenting the simulation results. In Section 2, we describe related work on image dehazing and highlight the advantages of this research in comparison to existing studies. In Section 3, we present the details of our proposed method. In Section 4, we show and compare our simulation results. In Section 5, the conclusions are given.

2. **Related Work.** In recent years, different approaches have been suggested to enhance the clarity of remote sensing images affected by haze. These methods can be categorized into three types: image enhancement-based methods [8], prior information-based methods [9], and learning-based methods [10]. Image enhancement-based methods can improve the clarity of remote sensing images, but the dehazed remote sensing image produced by this method is prone to excessive enhancement. Prior information-based approaches estimate the parameters of the atmospheric scattering model based on assumptions about it. While this method has certain dehazing effects, it may not effectively remove haze when the assumptions are inaccurate. Therefore, prior information-based approaches may not be suitable for reliable remote sensing image dehazing.

Learning-based methods for dehazing remote sensing images involve training network models with a large set of images to establish feature mappings between images with haze and images without haze. Liu et al. [11] proposed GridDehazeNet, a multi-scale network that includes attention mechanisms. In this method, information is efficiently exchanged between different scale feature maps, but the network suffers from poor generalization performance. Chen et al. [12] proposed GCANet, which incorporates a threshold sub-network for feature-weighted fusion based on feature importance. This method has good generalization capability for different types of images. However, it leads to edge blurring in output images due to the neglect of edge information. Zhao et al. [13] proposed RefinedNet, which breaks down dehazing into two sub-tasks: visibility restoration and authenticity improvement. Although this method avoids over-processing and preserves image authenticity, it can introduce noise. Wen et al. [14] proposed RSHazeNet, a dehazing method based on the minimum encoder and decoder architecture. This method can effectively restore the original colors of images but may cause the loss of fine details. Lu et al. [15] introduced the MixDehazeNet method, which can effectively handle unevenly distributed haze. However, images processed by this method tend to exhibit higher brightness.

In recent years, proposals for remote sensing image dehazing have emerged using generative adversarial networks, which is a type of deep learning technology. Generative adversarial networks are composed of a generator network and a discriminator network. The generator network's primary function is to dehaze remote sensing images, while the primary goal of the discriminator network is to discern between genuine images and artificially generated ones. Through the continuous competition between the generator and discriminator networks, the dehazing capability of the generator network for remote sensing images is enhanced. Compared to conventional learning-based image dehazing methods, dehazing performance is generally better with remote sensing image dehazing methods based on generative networks. Wang et al. [16] proposed the Cycle-SNSPGAN method, which introduces a novel cyclic self-perceptual loss function that does not require clear images to compute perceptual similarity. The method can effectively remove haze from images even when paired with clear images that are not available. Despite its usefulness, the method is susceptible to the problem of incomplete dehazing. Zheng et al. [17] proposed the Dehaze-AGGAN method. This method combines total variation loss with cycle consistency loss. The method is capable of effectively restoring the color characteristics

of the image, but it is susceptible to incomplete defogging. Liu et al. [18] introduced the AMEA-GAN method, which incorporates a horizontal visual enhancement module and an Amazon visual enhancement module. During the training process, these two modules work together to map each other, effectively removing haze. However, the images produced by this method are prone to over-enhancement issues. Chai et al. [19] proposed the PDD-GAN method, which uses images processed with a band-stop filter as the fourth channel of the input image, providing additional information for the dehazing network. Although this method can restore details accurately, it may cause distortions in colors. Jaisurya and Mukherjee [20] introduced the AGLC-GAN method, which employs a global-local consistent discriminator. This discriminator provides reliable feedback to the generator, enhancing its capability to remove unevenly distributed haze. However, this method introduces interference during the dehazing process, thereby lowering the quality of the dehazed images. Zhang et al. [21] introduced the GGADN method, which incorporates a guidance module into the generator network. This module enhances the details of feature maps at each layer of the generator network. While this method achieves high fidelity in detail restoration, it is prone to generating artifacts in the resulting images. Wang et al. [22] proposed the DFC-dehaze method, employing the Dehazeformer-t architecture for the generator and a local-global discriminator. Although this method effectively removes haze, it tends to produce color distortion in the generated images. Akhtar et al. [23] proposed the Mobile-Unet-GAN method, combining the UNet architecture with a generative adversarial network. While this method restores colors well, it suffers from the issue of detail loss in the generated images. Meng et al. [24] proposed DedustGAN, a weakly supervised method based on the Retinex model and unpaired image training. This method enhances the ability to dehaze real-world images but may result in color distortion. Chen et al. [25] proposed the ICycle-GAN method, embedding an iterative dehazing network into a cycle-consistent adversarial network. Although this method thoroughly removes haze, it tends to lose texture in the generated images.

Although previous methods have shown effectiveness in dehazing, the resulting images still exhibit certain issues. Image enhancement-based dehazing methods improve contrast and brightness, particularly in areas with dense haze. However, this can lead to the over-enhancement of certain details, resulting in visual distortions. To address this issue, we propose a residual attention module that adaptively adjusts feature weights, thereby mitigating the risk of excessive enhancement. Methods based on prior knowledge typically rely on atmospheric scattering models and certain empirical assumptions. If these assumptions do not accurately match the actual scene, it can result in information loss within the image. To address this issue, we designed a feature extraction module and utilized it to construct both the encoder and decoder, thereby enhancing the extraction of feature information from the image and minimizing information loss. Traditional learning-based image dehazing methods face limitations in capturing global contextual information and multi-scale texture features. These constraints hinder the model's ability to effectively capture complete details when processing images, often resulting in artifacts. To address this issue, we designed a multi-scale module that enhances the extraction of information across different scales, effectively reducing artifacts. Existing dehazing methods based on Generative Adversarial Networks (GANs) often suffer from color distortion in the generated images. To address this, we proposed a color feature extraction module that accurately extracts color information to reduce color distortion. Furthermore, we designed a novel discriminator network to enhance the dehazing capability of the generator.

3. **Methodology.**

To improve the visual clarity of remote sensing images affected by haze, we introduce a network based on GAN for image dehazing. This dehazing network

comprises two main networks: a generator network and a discriminator network. The primary objective of the generator network is to convert input hazy images into clear images. The discriminator network's purpose is to differentiate between the output images from the generator network and the real haze-free images. The generative network and the adversarial network engage in iterative adversarial training. This process encourages the generative network to produce more realistic images. Meanwhile, the adversarial network enhances its ability to discern generated images, thereby improving the overall quality of dehazing effects.

3.1. **Generator.** To improve the overall quality of remote sensing images, we have developed a generative network which is depicted in Figure 1. The network comprises five primary components: an encoder, a decoder, residual attention modules, a multi-scale module, and a color feature extraction module. We designed a feature extraction module, which is used to construct both the encoder and decoder. This module enhances the network's ability to extract crucial information from remote sensing images while reducing interference. Additionally, we designed residual attention modules and incorporated them into the feature fusion process of the encoder and decoder. These modules assign greater weights to important features of remote sensing images, reducing redundant information. We also designed a multi-scale module, which dynamically adjusts the focus on local and global features. Color distortion is a common issue in image dehazing networks. To tackle this issue, we design a color feature extraction module. In the following sections, detailed elucidations will be provided for each module.

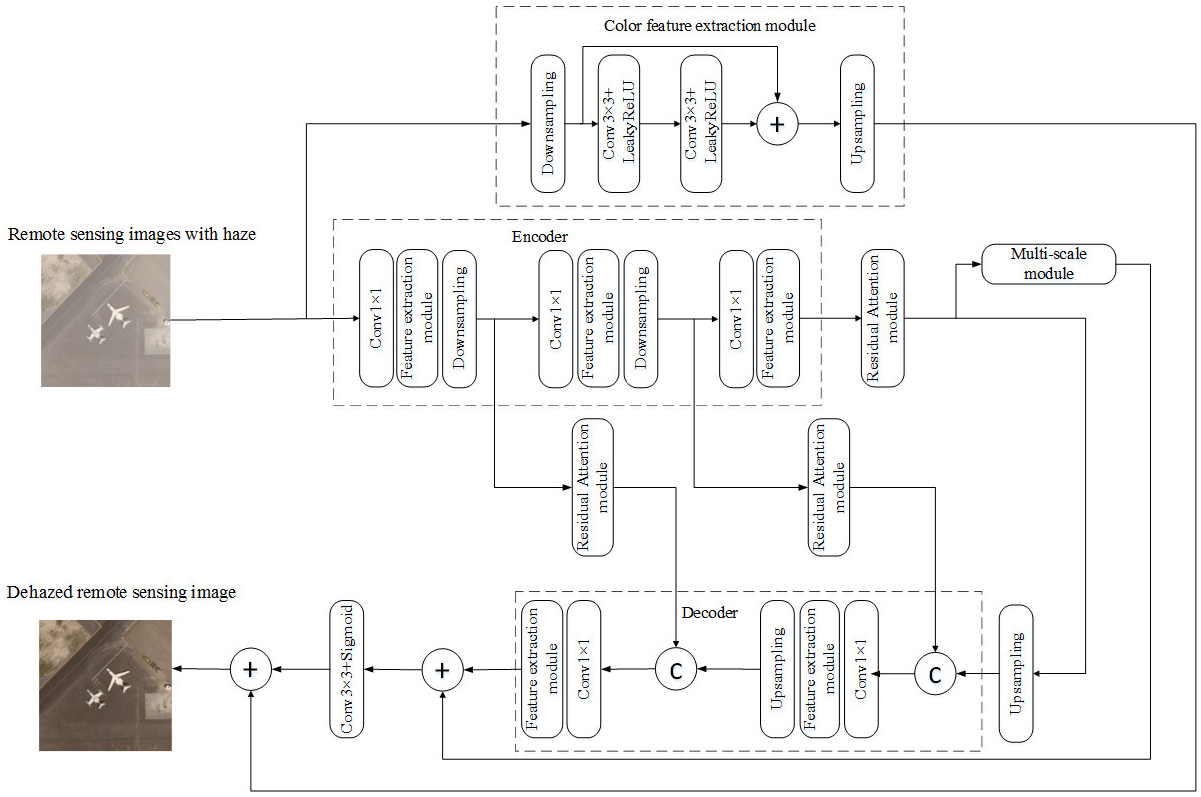

FIGURE 1. Proposed generative network

3.1.1. *Proposed feature extraction module.* The feature extraction module is depicted in Figure 2. Initially, the input feature maps undergo preliminary extraction through a 3×3 convolutional layer, followed by Batch Normalization, ReLU activation, and Dropout to

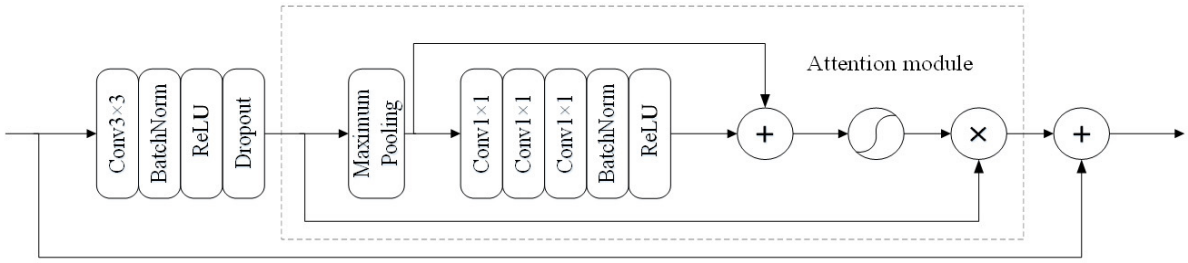

FIGURE 2. Proposed feature extraction module

mitigate overfitting. The feature maps produced by Dropout then pass through a max-pooling layer, followed by three consecutive 1×1 convolutional layers, Batch Normalization, ReLU activation, and a Sigmoid function to determine feature weights. These weights are applied element-wise to the input feature maps, resulting in weighted feature maps. Element-wise addition is then performed between the input and weighted feature maps, preserving the original information and minimizing information loss. The max-pooling layer extracts key information by downsampling the input, retaining only the most salient features. Three consecutive 1×1 convolutional layers extract feature information from remote sensing images. Batch Normalization and ReLU activation play pivotal roles in improving network stability and performance. Batch Normalization normalizes activations within each mini-batch, reducing internal covariate shift and speeding up training. ReLU introduces non-linearity, enabling the network to capture complex patterns while mitigating the vanishing gradient problem. Together, these components enhance feature extraction while minimizing interference.

3.1.2. *Proposed residual attention module.* The residual attention module is depicted in Figure 3. The module can adaptively weigh image features, enabling the network to focus on essential features and thereby enhancing feature utilization efficiency. The attention module consists of three branches, with the first branch including an average pooling layer followed by two 3×3 convolutions. These convolutions extract background information from remote sensing images. Skip connections are used in the first branch to minimize feature loss.

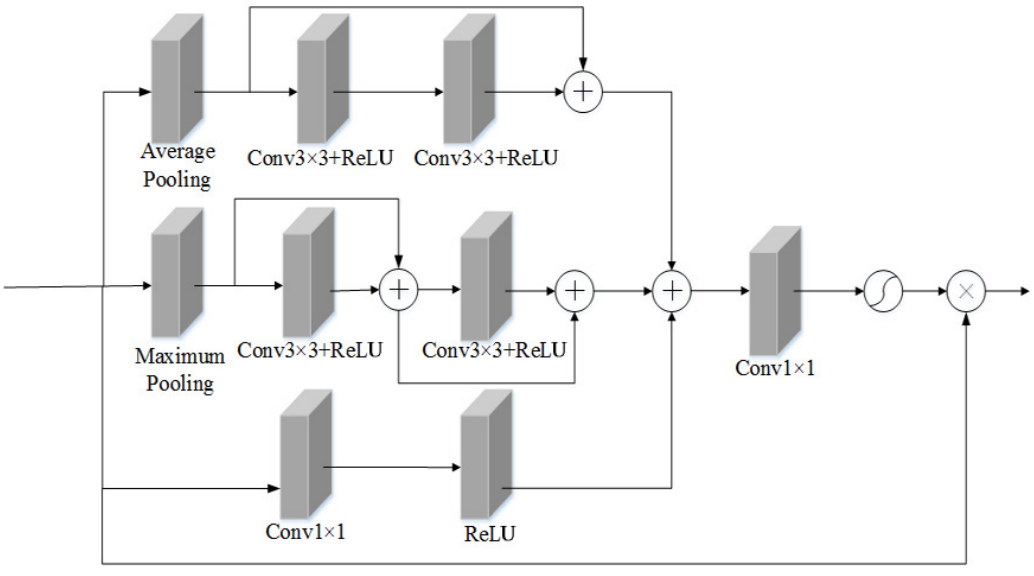

FIGURE 3. Proposed residual attention module

The feature maps generated by the first branch can be expressed as

$$c_1 = \phi\{Conv_{3\times3}[\phi(Conv_{3\times3}(Avg(X)))]\} \oplus Avg(X) \tag{1}$$

where X represents the input feature map of the attention module, ϕ represents the ReLU activation function, $Conv_{3\times3}$ signifies the 3×3 convolution operation, $\oplus$ represents element-wise addition, and the Avg indicates average pooling.

The second branch includes a max-pooling layer followed by two residual modules. The primary objective of the max-pooling layer is to extract texture information from remote sensing images. The residual modules consist of a 3×3 convolution and a ReLU activation function. The output feature maps of the second branch are represented as

$$y_1 = \phi\{Conv_{3\times3}[Max(X)]\} \oplus Max(X) \tag{2}$$

$$c_2 = \phi[Conv_{3\times3}(y_1)] \oplus y_1 \tag{3}$$

where X represents the input feature map of the attention module, ϕ denotes the ReLU activation function, $Conv_{3\times3}$ signifies the 3×3 convolution operation, $\oplus$ represents element-wise addition, Max indicates max-pooling, and y_1 represents the feature map of the output of the first residual module.

The third branch includes a 1×1 convolution followed by a ReLU activation function. This branch preserves the original feature information, reducing the loss of features during the extraction process. The output feature maps of the third branch are represented as

$$c_3 = \phi(Conv_{1\times1}(X)) \tag{4}$$

where $Conv_{1\times1}$ represents the 1×1 convolution operation. ϕ denotes the ReLU activation function.

The resultant feature maps generated by the residual attention module as a whole can be represented as

$$F(X) = X \otimes \sigma(Conv_{1\times1}(c_1 \oplus c_2 \oplus c_3)) \tag{5}$$

where $\otimes$ represents element-wise multiplication, $\oplus$ represents element-wise addition, c_1, c_2 and c_3 respectively represent the output feature maps of the first branch, the second branch, and the third branch, and σ represents Sigmoid activation.

3.1.3. *Proposed multi-scale module.* A larger receptive field is better for extracting global features, while a smaller receptive field is more effective for local features. To comprehensively extract features from remote sensing images, a multi-scale module has been developed, as illustrated in Figure 4. In this module, the number of channels is reduced from 256 to 128 using a 1×1 convolution. The max-pooling layer extracts texture information and highlights texture details, while the average pooling layer captures background information and emphasizes overall background characteristics. In order to improve information extraction, the feature maps are processed through three branches. The first branch uses a 3×3 dilated convolution with a dilation rate of 1, followed by BatchNorm and ReLU activation, producing 64 output channels. The second branch uses a 3×3 dilated convolution with a dilation rate of 2, followed by BatchNorm and ReLU activation, producing 32 output channels. The third branch uses a 3×3 dilated convolution with a dilation rate of 4, producing 32 output channels.

These branches extract features at different scales, enabling comprehensive image analysis. We concatenate the feature maps from the three branches, which capture features at different scales. The feature maps are initially reduced to a single channel using a 1×1 convolution, followed by Sigmoid activation to calculate the weights. Subsequently, the feature maps undergo two 1×1 convolutions, reducing the output channels to 64. The acquired weights are element-wise multiplied with the feature maps, highlighting important information while suppressing redundancy. Finally, adaptive average pooling is applied

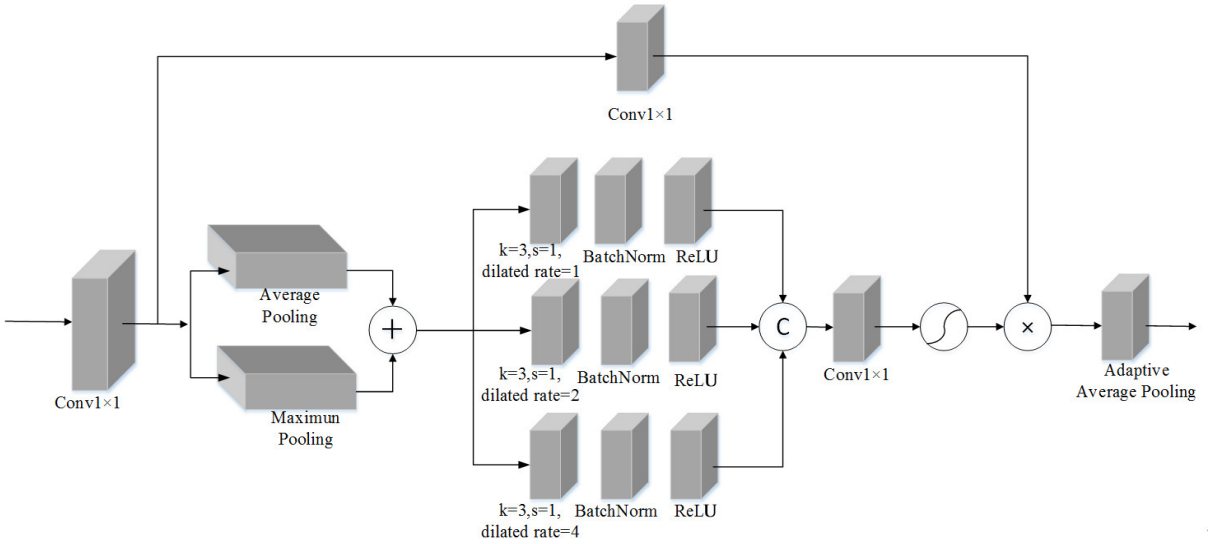

FIGURE 4. Proposed multi-scale module

to obtaining the output of the multi-scale module. This module enhances the network's ability to capture and process multi-scale features.

3.1.4. *Proposed color feature extraction module.* The traditional image dehazing networks often suffer from color distortion issues in the generated images. To tackle the issue of color distortion in dehazed images, we propose a color feature extraction module. As illustrated in Figure 1, this module consists of a downsampling layer, two 3×3 convolutions, two LeakyReLU activation functions, and an upsampling layer. The downsampling layer reduces interference in the input image while emphasizing its primary color features. The two skip-connected 3×3 convolutions enable the network to learn the distribution of colors in remote sensing images, thus preventing unnatural color transitions in the images. The LeakyReLU activation function enhances the network's ability to effectively adjust to diverse image variations. The upsampling operation restores the size of the feature maps to that of the original image, facilitating fusion with the subsequent decoder output features. Additionally, the upsampling operation enhances the image resolution, aiding in the recovery of color information lost due to the reduction in image size.

3.2. **Discriminator.** In the task of image dehazing, the discriminator network is trained adversarially with the generator network, continuously improving the generator to produce clearer and more realistic dehazed images. We propose a new discriminator network, illustrated in Figure 5, which consists of three modules. Each module comprises three branches. The first and second branches consist of 3×3 convolutions, BatchNorm, Dropout, and LeakyReLU activation functions. Here, the 3×3 convolutions extract features from the input image. BatchNorm enhances network stability. Dropout helps prevent overfitting. LeakyReLU activation functions accelerate network convergence. After concatenating the first and second branches, they pass through another 3×3 convolution to further extract features, enhancing the discriminator network's ability to distinguish between dehazed and haze-free images. The third branch is a 1×1 convolution that changes the channel number of the input feature map. By concatenating the feature maps obtained from the third branch with those from the first two branches, we capture a more comprehensive and rich set of image information. To extract more features from the image, we stack three such modules, enabling the network to better utilize feature information across different

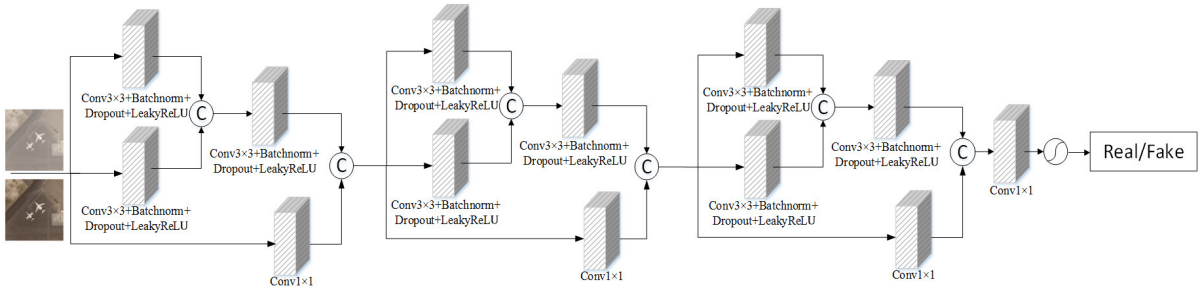

FIGURE 5. Proposed discriminator

layers and thus improve its performance in dehazing remote sensing images. Finally, we use a Sigmoid activation function to obtain the decision result.

3.3. **Loss function.** We present the loss function employed as follows:

$$L = \arg\min_{G}\max_{D} L_{cGAN}(G,D) + L_{L1}(G) + L_{pix} \tag{6}$$

where the loss function of the conditional generative adversarial network is as follows:

$$L_{cGAN}(G,D) = E_{x,y\sim p_{data}(x,y)}[\log D(x,y)] + E_{x\sim p_{data}(x,y),z\sim p_z(z)}[\log(1-D(x,G(x,z)))] \tag{7}$$

where x represents the input hazy remote sensing image, y represents the generated dehazed image, and z represents the noise input to the generator.

The $L_{L1}(G)$ measures the difference between the prediction of the model and the ground truth label. It is described as follows:

$$L_{L1}(G) = \frac{1}{CHW}\sum_{c=1}^{C}\sum_{v=1}^{H}\sum_{u=1}^{W}\lambda_c\left|I_{gt}^{(u,v,c)} - G(I_{in})^{(u,v,c)}\right|_1 \tag{8}$$

where I_{in} is the input hazy image, $G(I_{in})$ is the dehazed image output by the generative network, I_{gt} is the clear haze-free image, and λ_c is the contribution weight of each channel to the loss. C, H, W denote the number of channels, height, and width of the image, respectively.

The pixel loss function is used to measure the pixel-wise difference between the generator-generated image and the haze-free image. It is described as follows:

$$L_{pix} = \sum_{i=1}^{m}(I_{gt} - I_{pre})^2 \tag{9}$$

where I_{pre} is the generated image by generator. I_{gt} is the haze-free image.

4. **Simulation and Discussion.** The proposed method is compared with Cycle-SNSP-GAN, RSHazeNet, MixDehazeNet, GCANet, and DedustGAN methods. For quantitative evaluation, we employ the PSNR [26], MSE [27], and SSIM [28] metrics to assess the quality of the images generated by six methods. The PSNR is defined as follows:

$$PSNR = 10 \times \log_{10}\left(\frac{MAX^2}{MSE}\right) \tag{10}$$

where MAX represents the maximum pixel value of the image generated by the dehazing network. MSE represents the mean squared error between the generated dehazed image and the haze-free image. A higher $PSNR$ value suggests a stronger resemblance between the output image generated by the dehazing method and the original clear image, thereby indicating superior image quality.

The *MSE* is described as follows:

$$MSE = \frac{1}{mn}\sum_{i=1}^{m}\sum_{j=1}^{n}\left(I(i,j) - \hat{I}(i,j)\right)^2 \tag{11}$$

where m represents the height of the image, and n represents the width of the image. $I(i,j)$ represents the pixel value at the position (i,j) in the haze-free image, while $\hat{I}(i,j)$ represents the pixel value at the position (i,j) in the image generated by the dehazing method. A smaller value of *MSE* indicates a smaller difference between the dehazed image and the original clear image, indicating higher effectiveness of the dehazing method.

The *SSIM* is described as follows:

$$SSIM(x,y) = \frac{(2u_x u_y + c_1)(2\delta_{xy} + c_2)}{\left(u_x^2 + u_y^2 + c_1\right)\left(\delta_x^2 + \delta_y^2 + c_2\right)} \tag{12}$$

where u_x and u_y represent the means of the dehazed image and the haze-free image, respectively. δ_x^2 and δ_y^2 denote the variances of the dehazed image and the haze-free image. δ_{xy} is the covariance between the dehazed image and the haze-free image. $c_1 = k_1 L$ and $c_2 = k_2 L$ are constants used to prevent instability caused by division by zero. L represents the dynamic range of pixel values. k_1 and k_2 are constants; we set $k_1 = 0.01$ and $k_2 = 0.03$. A larger *SSIM* value suggests that the dehazed image exhibits a higher resemblance to the haze-free image.

We compiled a dataset based on the UC Merced Land Use dataset [29] to train and evaluate the remote sensing dehazing network model. The UC Merced Land Use dataset comprises 21 distinct scene categories, each encompassing 100 images. Employing the atmospheric scattering model, we generated 2100 hazy remote sensing images. By pairing these synthetic images with their corresponding original counterparts, we obtained a total of 2100 matched image pairs. Among them, we selected 1680 pairs for training purposes while allocating the remaining 420 pairs for testing.

4.1. **Simulation on synthetic remote sensing images.** We randomly selected six synthetic hazy remote sensing images for dehazing. Our proposed method, along with Cycle-SNSPGAN, RSHazeNet, MixDehazeNet, GCANet, and DedustGAN methods is employed to perform the dehazing process on these images. Figure 6 illustrates both the hazy images and their corresponding dehazed counterparts. The first column of the figure showcases the synthetic hazy images while the last column exhibits the haze-free images. The remaining six columns sequentially present the dehazed images obtained by Cycle-SNSPGAN, RSHazeNet, MixDehazeNet, GCANet, DedustGAN, and our proposed method.

In the first row, the dehazed remote sensing images obtained by the Cycle-SNSPGAN and DedustGAN methods exhibit a problem of color bias towards white. The dehazed remote sensing image obtained by the RSHazeNet method suffers from a problem of low brightness. The dehazed remote sensing images obtained by the MixDehazeNet and GCANet methods encounter a problem of excessive brightness. In the second row, the dehazed remote sensing images from Cycle-SNSPGAN and DedustGAN methods exhibit a problem of color bias towards gray. The dehazed remote sensing image obtained by the RSHazeNet method suffers from a problem of color bias towards dark. The dehazed remote sensing image obtained by the MixDehazeNet method encounters a problem of excessive brightness. The dehazed remote sensing image obtained by the GCANet method shows artifacts. In the third row, the dehazed remote sensing images obtained by the Cycle-SNSPGAN and DedustGAN methods exhibit a grayish color bias. The dehazed image obtained by the RSHazeNet method shows issues of excessive enhancement. The

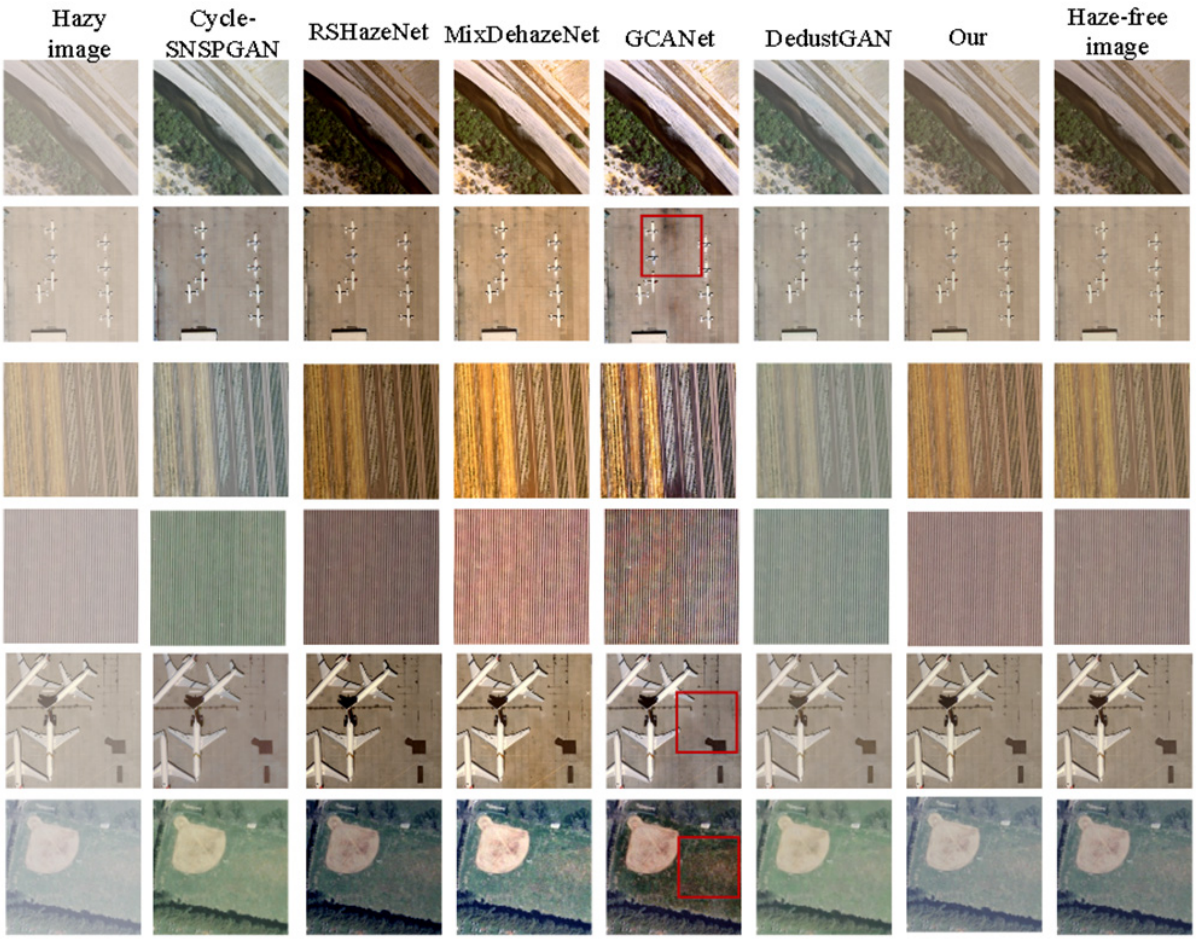

FIGURE 6. Outcomes of different dehazing methods applied to synthesized hazy remote sensing visuals

dehazed remote sensing images obtained by the MixDehazeNet method and GCANet method exhibit problems of color oversaturation.

In the fourth row, the remote sensing images obtained by the Cycle-SNSPGAN and DedustGAN methods exhibit a greenish color bias. The image obtained by the RSHazeNet method shows a problem of low brightness, which can lead to the ineffective identification of important information in the image. The image obtained by the MixDehazeNet method exhibits a problem of high brightness. The image obtained by the GCANet method shows numerous artifacts. In the fifth row, the dehazed remote sensing image obtained by the Cycle-SNSPGAN method exhibits a problem of color bias towards gray. The dehazed remote sensing image obtained by the RSHazeNet method suffers from a problem of color bias towards dark. The dehazed remote sensing image obtained by the MixDehazeNet method encounters a problem of excessive brightness. The dehazed remote sensing image obtained by the GCANet method shows artifacts. The dehazed remote sensing image obtained by the DedustGAN method has residual haze issues. In the sixth row, the dehazed remote sensing images obtained by the Cycle-SNSPGAN and DedustGAN methods exhibit a problem of color bias towards light. The dehazed remote sensing image obtained by the RSHazeNet method suffers from a problem of color bias towards blue. The dehazed image obtained by the MixDehazeNet method encounters a problem of excessive brightness. The dehazed image obtained by the GCANet method shows red artifacts.

To objectively assess the dehazing capabilities of different methods, we compared Cycle-SNSPGAN, RSHazeNet, MixDehazeNet, GCANet, DedustGAN methods, and our method using three evaluation metrics: PSNR, SSIM, and MSE on the test dataset, as shown in Table 1. The PSNR values for Cycle-SNSPGAN, RSHazeNet, MixDehazeNet, GCANet, DedustGAN, and our method are 26.4907, 28.6025, 26.1548, 22.5232, 31.8389, and 33.4842, respectively. Our method achieved the highest PSNR value, indicating superior quality in the dehazed remote sensing images it produces. The SSIM values for Cycle-SNSPGAN, RSHazeNet, MixDehazeNet, GCANet, DedustGAN, and our method are 0.9505, 0.9779, 0.9623, 0.9274, 0.9749, and 0.9854, respectively. Our method achieved the highest SSIM value, suggesting that its dehazed remote sensing images closely resemble haze-free images in terms of brightness and contrast. Regarding MSE values, Cycle-SNSPGAN, RSHazeNet, MixDehazeNet, GCANet, DedustGAN, and our method yield 0.0047, 0.0031, 0.0040, 0.0094, 0.0011, and 0.0010, respectively. Our proposed method exhibits the smallest MSE value, indicating superior dehazing performance with minimal difference between dehazed and haze-free images. In summary, our proposed method outperforms others in dehazing remote sensing images.

TABLE 1. Comparison of synthetic remote sensing images

Method	PSNR	SSIM	MSE
Cycle-SNSPGAN	26.4907	0.9505	0.0047
RSHazeNet	28.6025	0.9779	0.0031
MixDehazeNet	26.1548	0.9623	0.0040
GCANet	22.5232	0.9274	0.0094
DedustGAN	31.8389	0.9749	0.0011
Our method	33.4842	0.9854	0.0010

4.2. **Simulation on real remote sensing images.** To evaluate the dehazing capabilities of various approaches on real remote sensing images, we conducted experiments on the RRSD300 dataset, which consists of 300 real hazy remote sensing images. From this dataset, we randomly selected four real hazy remote sensing images as test samples. Figure 7 showcases both the original hazy remote sensing images and the corresponding dehazed images obtained by various dehazing methods. The first column exhibits real hazy remote sensing images. The second to seventh columns respectively exhibit the dehazed remote sensing images generated by employing Cycle-SNSPGAN method, RSHazeNet method, MixDehazeNet method, GCANet method, DedustGAN method, and our proposed method.

In the first row, dehazed remote sensing images from Cycle-SNSPGAN and DedustGAN methods exhibit a yellowish color cast. The dehazed remote sensing image obtained by the RSHazeNet method results in detail loss. The MixDehazeNet method produces an excessively bright image. GCANet method generates image with a blackish color bias. In the second row, dehazed remote sensing images from Cycle-SNSPGAN and DedustGAN methods exhibit a greenish color cast. The RSHazeNet method leads to detail blurring. The MixDehazeNet method produces an excessively bright image. GCANet method generates an image with a blackish color bias. In the third row, the dehazed image from Cycle-SNSPGAN exhibits a yellowish color cast. The RSHazeNet and MixDehazeNet methods result in low brightness levels for their respective output images. GCANet method shows artifacts. In the fourth row, the dehazed remote sensing image from the Cycle-SNSPGAN method displays a greenish color bias. The image from the RSHazeNet method exhibits

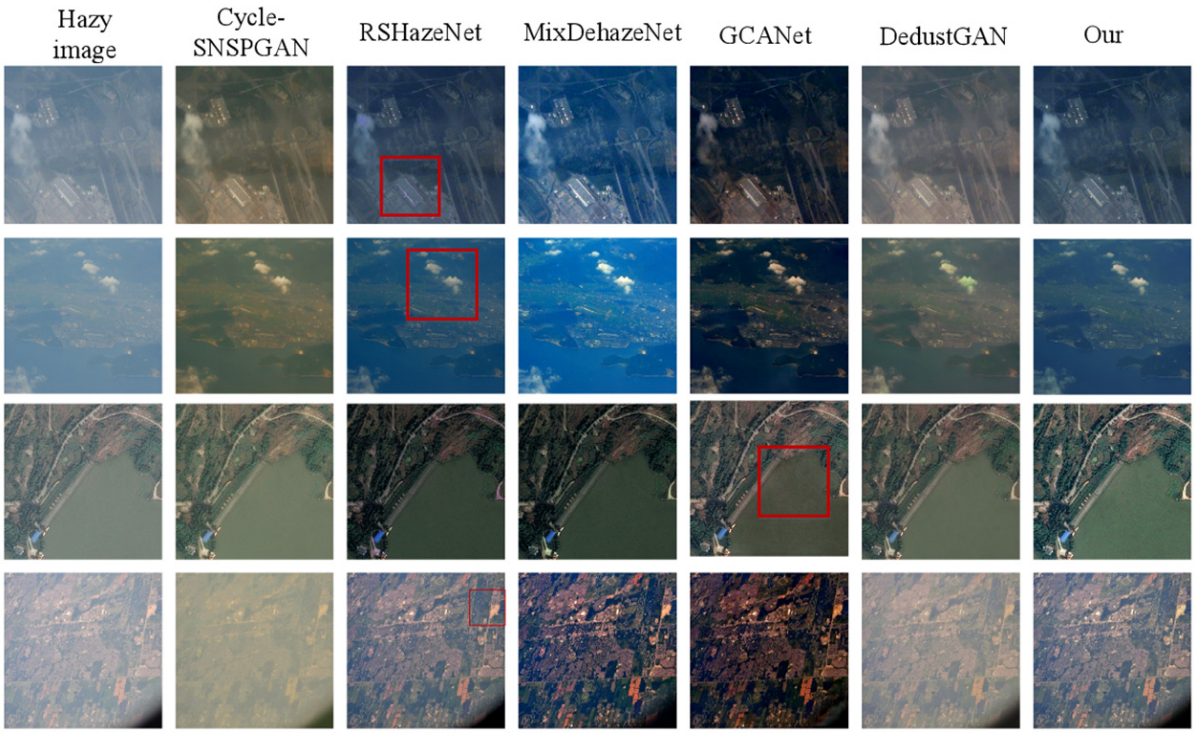

FIGURE 7. Outcomes of different dehazing methods applied to real remote sensing visuals

color distortion in detail. Conversely, the dehazed remote sensing image from the MixDehazeNet method demonstrates excessive enhancement. Meanwhile, the image produced by the GCANet method reveals a reddish color bias. Lastly, the dehazed remote sensing image generated by the DedustGAN method contains residual haze.

To objectively analyze the dehazing capabilities of different methods on the real remote sensing images, we compared the Cycle-SNSPGAN method, RSHazeNet method, MixDehazeNet method, GCANet method, DedustGAN method, and our method using three evaluation metrics: PIQE [30], MetaIQA [31], and BRISQUE [32] on the RRSD300 dataset. The results are presented in Table 2. Average PIQE and average BRISQUE scores of the images generated by our proposed method are the lowest, and the average MetaIQA score is the highest. This indicates that compared to the other comparative methods, the images produced by our proposed network have the best quality.

TABLE 2. Comparison of real remote sensing images

Method	PIQE	MetaIQA	BRISQUE
Cycle-SNSPGAN	17.0532	0.2609	30.5176
RSHazeNet	25.3699	0.2560	38.4824
MixDehazeNet	14.9590	0.2554	30.6602
GCANet	15.2966	0.2449	31.2228
DedustGAN	27.7623	0.2572	37.0476
Our method	11.3699	0.2621	29.5038

4.3. **Ablation experiment.** The impact of different modules in the network on the image dehazing task was examined by removing the feature extraction module, multi-scale module, residual attention module, and color feature extraction module, resulting

in four distinct configurations of dehazing networks. These four networks were employed to dehaze all images in the test dataset, and the corresponding test results are presented in Table 3. The average PSNR values for the dehazing networks without the feature extraction module, without the multi-scale module, without the residual attention module, and without the color feature extraction module were determined as 29.8047, 29.4680, 29.8830, and 30.4004, respectively. Similarly, their average SSIM values were found to be 0.9734, 0.9682, 0.9759, and 0.9783, respectively, and their average MSE values stood at 0.0022, 0.0028, 0.0018, and 0.0015, respectively. Based on this analysis, it can be concluded that among all modules, the multi-scale module plays a pivotal role within the dehazing network, whereas minimal influence is demonstrated by the color feature extraction module.

Table 3. The test results for different modules

Method	PSNR	SSIM	MSE
No_feature extraction module	29.8047	0.9734	0.0022
No_multi-scale module	29.4680	0.9682	0.0028
No_residual attention module	29.8830	0.9759	0.0018
No_color feature extraction module	30.4004	0.9783	0.0015

5. **Conclusions.** The paper initially introduces the design of several key modules: the feature extraction module, residual attention module, multi-scale module, and color feature extraction module. Subsequently, these modules are integrated to form a generative network customized to enhance visibility in remote sensing images affected by haze. Additionally, a discriminative network is devised to enhance the dehazing performance of the generative network. The proposed method undergoes testing on both synthetic and real remote sensing image datasets, with comparisons drawn against Cycle-SNSPGAN, RSHazeNet, MixDehazeNet, GCANet, and DedustGAN methods. On the synthetic remote sensing images dataset, our method attains the highest average PSNR, SSIM, and the lowest average MSE when compared to other methods. On the real remote sensing images dataset, our method achieves the highest average MetaIQA, lowest average PIQE, and lowest average BRISQUE in comparison to other methods. These findings suggest that the dehazed images produced by our method closely resemble haze-free images, showcasing superior dehazing performance over other methods. However, despite achieving commendable dehazing results, our proposed method entails a relatively complex network architecture, resulting in prolonged training and testing durations. In future endeavors, we aim to streamline the network structure to alleviate complexity, expedite network training, and enhance dehazing efficiency.

Acknowledgment. This work was supported by the Science and Technology Research Project of Jilin Provincial Department of Education (JJKH20230125KJ).

REFERENCES

[1] J. Sun, Y. Wang, Y. Sun and F. Jin, Fault diagnosis method of migration learning based on antagonism generation network, *International Journal of Innovative Computing, Information and Control*, vol.19, no.6, pp.1953-1968, 2023.

[2] X. Xu and Q. Huang, Depth map restoration algorithm based on improved super-resolution and FMM by using weight function, *International Journal of Innovative Computing, Information and Control*, vol.18, no.2, pp.577-590, 2022.

[3] K. Malathi, S. N. Shruthi, N. Madhumitha and S. Sreelakshmi, Medical data integration and interoperability through remote monitoring of healthcare devices, *Journal of Wireless Mobile Networks, Ubiquitous Computing, and Dependable Applications (JoWUA)*, vol.15, pp.60-72, 2024.
[4] Q. Zhu, X. Guo, Z. Li and D. Li, A review of multi-class change detection for satellite remote sensing imagery, *Geo-Spatial Information Science*, vol.27, pp.1-15, 2024.
[5] M. Feinstein, D. Katz, S. Demaria and I. S. Hofer, Remote monitoring and artificial intelligence: Outlook for 2050, *Anesthesia & Analgesia*, vol.138, pp.350-357, 2024.
[6] X. Zhang, Q. Su, P. Xiao, W. Wang, Z. Li and G. He, FlipCAM: A feature-level flipping augmentation method for weakly supervised building extraction from high-resolution remote sensing imagery, *IEEE Transactions on Geoscience and Remote Sensing*, vol.62, pp.1-17, 2024.
[7] Y. He, C. Li and X. Li, Remote sensing image dehazing using heterogeneous atmospheric light prior, *IEEE Access*, vol.11, pp.18805-18820, 2023.
[8] Y. Song, Z. He, H. Qian and X. Du, Vision transformers for single image dehazing, *IEEE Transactions on Image Processing*, vol.32, pp.1927-1941, 2023.
[9] Z. Zhang, C. Yan, S. Zhang, L. Bu and M. Deng, A multimodal feature fusion image dehazing method with scene depth prior, *IET Image Processing*, vol.17, pp.3079-3094, 2023.
[10] V. A. Devi and E. Bhuvaneswari, Single image dehazing using a channel and pixel attention network, *2024 2nd International Conference on Emerging Trends in Information Technology and Engineering*, pp.1-7, 2024.
[11] X. Liu, Y. Ma, Z. Shi and J. Chen, GridDehazeNet: Attention-based multi-scale network for image dehazing, *2019 IEEE/CVF International Conference on Computer Vision (ICCV)*, Seoul, Korea, pp.7313-7322, 2019.
[12] D. Chen, M. He, Q. Fan, J. Liao, L. Zhang, D. Hou and G. Hua, Gated context aggregation network for image dehazing and deraining, *2019 IEEE Winter Conference on Applications of Computer Vision (WACV)*, Waikoloa, HI, USA, pp.1375-1383, 2019.
[13] S. Zhao, L. Zhang, Y. Shen and Y. Zhou, RefineDNet: A weakly supervised refinement framework for single image dehazing, *IEEE Transactions on Image*, vol.10, pp.989-995, 2019.
[14] Y. Wen, T. Gao, Z. Li, J. Zhang and T. Chen, Encoder-minimal and decoder-minimal framework for remote sensing image dehazing, *2024 IEEE International Conference on Acoustics, Speech and Signal Processing (ICASSP 2024)*, Seoul, Korea, pp.36-40, 2024.
[15] L. Lu, Q. Xing, D. Chu and B. Xu, MixDehazeNet: Mix structure block for image dehazing network, *2024 International Joint Conference on Neural Networks (IJCNN)*, pp.1-10, 2014.
[16] Y. Wang, X. Yan, D. Guan, M. Wei and Y. Chen, Cycle-SNSPGAN: Towards real-world image dehazing via cycle spectral normalized soft likelihood estimation patch GAN, *IEEE Transactions on Intelligent Transportation Systems*, vol.23, pp.20368-20382, 2022.
[17] Y. Zheng, J. Su, S. Zhang, M. Tao and L. Wang, Dehaze-AGGAN: Unpaired remote sensing image dehazing using enhanced attention-guide generative adversarial networks, *IEEE Transactions on Geoscience and Remote Sensing*, vol.60, 5630413, 2022.
[18] Y. Liu, H. Al-Shehari and H. Zhang, Attention mechanism enhancement algorithm based on cycle consistent generative adversarial networks for single image dehazing, *Journal of Visual Communication and Image Representation*, vol.83, 103434, 2022.
[19] X. Chai, J. Zhou, H. Zhou and J. Lai, PDD-GAN: Prior-based GAN network with decoupling ability for single image dehazing, *Proc. of the 30th ACM International Conference on Multimedia*, pp.5952-5960, 2022.
[20] R. S. Jaisurya and S. Mukherjee, AGLC-GAN: Attention-based global-local cycle-consistent generative adversarial networks for unpaired single image dehazing, *Image and Vision Computing*, vol.140, 104859, 2023.
[21] J. Zhang, Q. Dong and W. Song, GGADN: Guided generative adversarial dehazing network, *Soft Computing*, vol.27, pp.1731-1741, 2023.
[22] S. Wang, X. Mei, P. Kang, Y. Li and D. Liu, DFC-dehaze: An improved cycle-consistent generative adversarial network for unpaired image dehazing, *The Visual Computer*, vol.40, pp.1-12, 2023.
[23] M. S. Akhtar, A. Ali and S. S. Chaudhuri, Mobile-UNet GAN: A single-image dehazing model, *Signal, Image and Video Processing*, vol.18, pp.275-283, 2023.
[24] X. Meng, J. Huang, Z. Li, C. Wang, S. Teng and A. Grau, DedustGAN: Unpaired learning for image dedusting based on Retinex with GANs, *Expert Systems with Applications*, vol.243, 122844, 2024.
[25] Y. Chen, H. Lin, W. Zhang, W. Chen, Z. Zhou, H. Chen and G. Xu, ICycle-GAN: Improved cycle generative adversarial networks for liver medical image generation, *Biomedical Signal Processing and Control*, vol.92, 06100, 2024.

[26] H. R. Sheikh, M. F. Sabir and A. C. Bovik, A statistical evaluation of recent full reference image quality assessment algorithms, *IEEE Transactions on Image Processing*, vol.15, pp.3440-3451, 2006.
[27] A. N. Omara, H. Farouk and S. A. Mohamed, NOMP: A new sparse solution to enhance the SSIM levels of OMP-based encoded images, *IEEE Access*, vol.10, pp.46067-46081, 2022.
[28] H. Gao, S. Li and R. Dian, Hyperspectral and multispectral image fusion via self-supervised loss and separable loss, *IEEE Transactions on Geoscience and Remote Sensing*, vol.60, 5537712, 2022.
[29] Y. Yang and S. Newsam, Bag-of-visual-words and spatial extensions for land-use classification, *ACM SIGSPATIAL International Conference on Advances in Geographic Information Systems (ACM GIS)*, pp.270-279, 2010.
[30] A. K. Moorthy and A. C. Bovik, Blind image quality assessment: From natural scene statistics to perceptual quality, *IEEE Transactions on Image Processing*, vol.20, pp.3350-3364, 2011.
[31] H. Zhu, L. Li, J. Wu, W. Dong and G. Shi, MetaIQA: Deep meta-learning for no-reference image quality assessment, *Proc. of the IEEE/CVF Conference on Computer Vision and Pattern Recognition*, pp.14143-14152, 2020.
[32] A. Mittal, A. K. Moorthy and A. C. Bovik, Blind/referenceless image spatial quality evaluator, *2011 Conference Record of the 45th Asilomar Conference on Signals, Systems and Computers (ASILOMAR)*, pp.723-727, 2011.

Author Biography

Liquan Zhao received the B.Eng. degree from Harbin University of Science and Technology, China, in 2005; the Ph.D. degree in Communication and Information System, from Harbin Engineering University, China, in 2009.

He is currently a full-time professor at the College of Electric Engineering, Northeast Electric Power University, China. His research interests include artificial intelligence and object detection. He has published over 40 papers in journals and conferences.

Yuqing Qin received the B.Eng. degree in Communication Engineering from Northeast Electric Power University China, in 2021. She is studying for a master's degree in Northeast Electric Power University, Jilin, China. Her main research interests include deep learning and generative adversarial networks.

Yanfei Jia received the B.Eng. degree from Harbin University of Science and Technology, China, in 2005; the Ph.D. degree in Communication and Information System, from Harbin Engineering University, China, in 2018.

She is currently a full-time associate professor at the College of Electric and Information Engineering, Beihua University, China. Her research interests include artificial intelligence, wireless sensor network, and blind source separation. She has published over 10 papers in journals and conferences.